

BrainWave: A Brain Signal Foundation Model for Clinical Applications

Zhizhang Yuan¹, Fanqi Shen¹, Meng Li^{2,3}, Yuguo Yu^{4,5},
Chenhao Tan⁶, Yang Yang^{1*}

¹Computer Science and Technology, Zhejiang University, Hangzhou, Zhejiang, China.

²Shanghai Institute of Microsystem and Information Technology, Chinese Academy of Sciences, Shanghai, China.

³INSIDE Institute for Biological and Artificial Intelligence, Shanghai, China.

⁴Research Institute of Intelligent and Complex Systems, State Key Laboratory of Medical Neurobiology and MOE Frontiers Center for Brain Science, and Institute of Science and Technology for Brain-Inspired Intelligence, Fudan University, Shanghai, China.

⁵Shanghai Artificial Intelligence Laboratory, Fudan University, Shanghai, China.

⁶University of Chicago, Chicago, Illinois, USA.

*Corresponding author(s). E-mail(s): yangya@zju.edu.cn;

Contributing authors: zhizhangyuan@zju.edu.cn; fanqishen@zju.edu.cn; li.meng@mail.sim.ac.cn; yuyuguo@fudan.edu.cn; chenhao@uchicago.edu;

Abstract

Neural electrical activity is fundamental to brain function, underlying a range of cognitive and behavioral processes, including movement, perception, decision-making, and consciousness. Abnormal patterns of neural signaling often indicate the presence of underlying brain diseases. The variability among individuals, the diverse array of clinical symptoms from various brain disorders, and the limited availability of diagnostic classifications, have posed significant barriers to formulating reliable model of neural signals for diverse application contexts. Here, we present BrainWave, the first foundation model for both invasive and non-invasive neural recordings, pretrained on more than 40,000 hours of electrical brain recordings (13.79 TB of data) from approximately 16,000 individuals. Our

analysis show that BrainWave outperforms all other competing models and consistently achieves state-of-the-art performance in the diagnosis and identification of neurological disorders. We also demonstrate robust capabilities of BrainWave in enabling zero-shot transfer learning across varying recording conditions and brain diseases, as well as few-shot classification without fine-tuning, suggesting that BrainWave learns highly generalizable representations of neural signals. We hence believe that open-sourcing BrainWave will facilitate a wide range of clinical applications in medicine, paving the way for AI-driven approaches to investigate brain disorders and advance neuroscience research.

Keywords: foundation model, brain signals, EEG, iEEG

1 Introduction

Electrical brain recordings, capturing the intricate patterns of the brain’s electrical activities, are essential in advancing our understanding of brain across scientific domains [1–7]. In particular, they can be used to identify medical conditions and diagnose neurological disorders, and are thus essential for addressing major global health challenges in developing nations [8, 9]. Scalp electroencephalography (EEG) and intracranial electroencephalography (iEEG) are two primary methods to conduct these types of recordings. EEG is non-invasive and economical viable, and has thus been used in diverse applications [10–14]. In contrast, iEEG offers high signal fidelity and spatial resolution [15], but the invasive nature limits its applicability to only the most severe patient cases and restricted scenarios. Due to the distinct features of EEG and iEEG data, such as different acquisition rates and notable variations in channel numbers [16–18], studies have so far investigated them separately. We hypothesize that combining EEG and iEEG data can offer information that are not only rich in detail but also highly generalizable across diverse neural electrical activities, and develop a pioneering foundational model, BrainWave, for both EEG and iEEG data. BrainWave learns robust representations that achieve the state-of-art performance in a wide range of tasks, demonstrating the synergy of EEG and iEEG data for the first time.

BrainWave overcomes a suite of inherent challenges in conventional supervised artificial intelligence (AI) models used for the analysis of brain signals. First, BrainWave leverages self-supervised training, circumventing the need for large-scale, high-quality manual labeling. In clinical applications, the process of brain data annotation is labor-intensive and reliant on specialized expertise [19–21], exemplified by the need for multi-day monitoring for epilepsy patients [22] and the clinical experts’ capacity to annotate only tens of seconds of data in a single work period. Second, BrainWave provides much-needed generalization at two levels that were not possible in supervised training, which requires an understanding of fundamental and general patterns in brain signals. Individual variability in brain neural activities, a consequence of each person’s distinct brain structure and functional behaviors [23], leads to markedly different brain recording patterns [24]. This diversity hinders the generalizability of supervised AI models, as they often struggle to extend the insights gained from a subset of patients

to a broader population, due to significant differences across individuals, as well as variability that changes with different behavioral states. Moreover, there are numerous types of brain-related diseases with various underlying mechanisms [25–28], and even a single disease may present with multiple subtypes [29]. Supervised AI models are also task-specific and fail to address a diverse range of tasks using brain signals [24, 30–37], indicating that they do not actually “understand” brain signals.

While prior work has attempted to build foundation models for brain signals [38–43], BrainWave offered unique technical contributions by building the largest dataset of electrical brain recordings and developing novel techniques to integrate EEG and iEEG data for the first time. As illustrated in Figure 1a, we collected a total of 13.79 TB of combined EEG and iEEG data over a duration of 40,907 hours, which serves as the foundation for pretraining BrainWave. The data were obtained from 15,997 individuals, including both healthy individuals and those with various brain disorders, spanning an age range from infancy (< 1 year) to over 90 years old. In the pretraining stage, we adopt a masked modeling strategy that reconstructs the time-frequency representations of the masked patches (Fig. 1b). Unlike previous works that uniformly resampled data to a common sampling rate [44–46], the designed embedding layer of BrainWave can adapt to different temporal resolutions, which enhanced the data scalability and provided the model with stronger generalization capabilities. We also employed a channel count-agnostic approach to capture the inter-channel relationships. Empowered by growing datasets and advances in model design, BrainWave exhibited highly robust pretrained representations and excellent transfer learning capabilities (Fig. 1c).

We systematically evaluated BrainWave and observed its exceptional performance across different settings, including cross-subject (Fig. 2a and b), cross-hospital (Fig. 2c) and cross-subtype (Fig. 2d) tasks, which attests to its strong generalization capabilities. Additionally, its proficiency in few-shot classification (Fig. 3) highlights its adaptability in learning from limited data. We also demonstrated the effectiveness of joint pretraining by leveraging both invasive and non-invasive neural data (Fig. 4a-c) and found that it achieved superior performance by learning more generalizable representations (Fig. 4e) and richer semantic information (Supplementary Tables 38 and 39). To comprehensively assess the capabilities of BrainWave as a foundation model for electrical brain recordings in healthcare scenarios, we constructed a benchmark comprising 15 different datasets. BrainWave is compared against the previous state-of-the-art foundation models that are publicly available, including LaBraM [44], BrainBERT [46] and MOMENT [47]. Figure 1d summarizes the overall results of BrainWave compared with other methods, in which BrainWave attains consistently state-of-the-art performance on all the 28 experiments, with significant improvement ($p < 0.001$) over the second-best method in 24 experiments, showing the versatility of BrainWave in a wide array of tasks for brain recordings in healthcare. To investigate the effectiveness of joint pretraining with both invasive and non-invasive neural data, we separately pretrained two model variants using EEG and iEEG data under the condition of maintaining other pretraining settings constant, and compared them across all experimental settings (Fig. 4a-d). The results show that BrainWave outperforms other variants in diverse tasks and experimental setups, marking it as the first

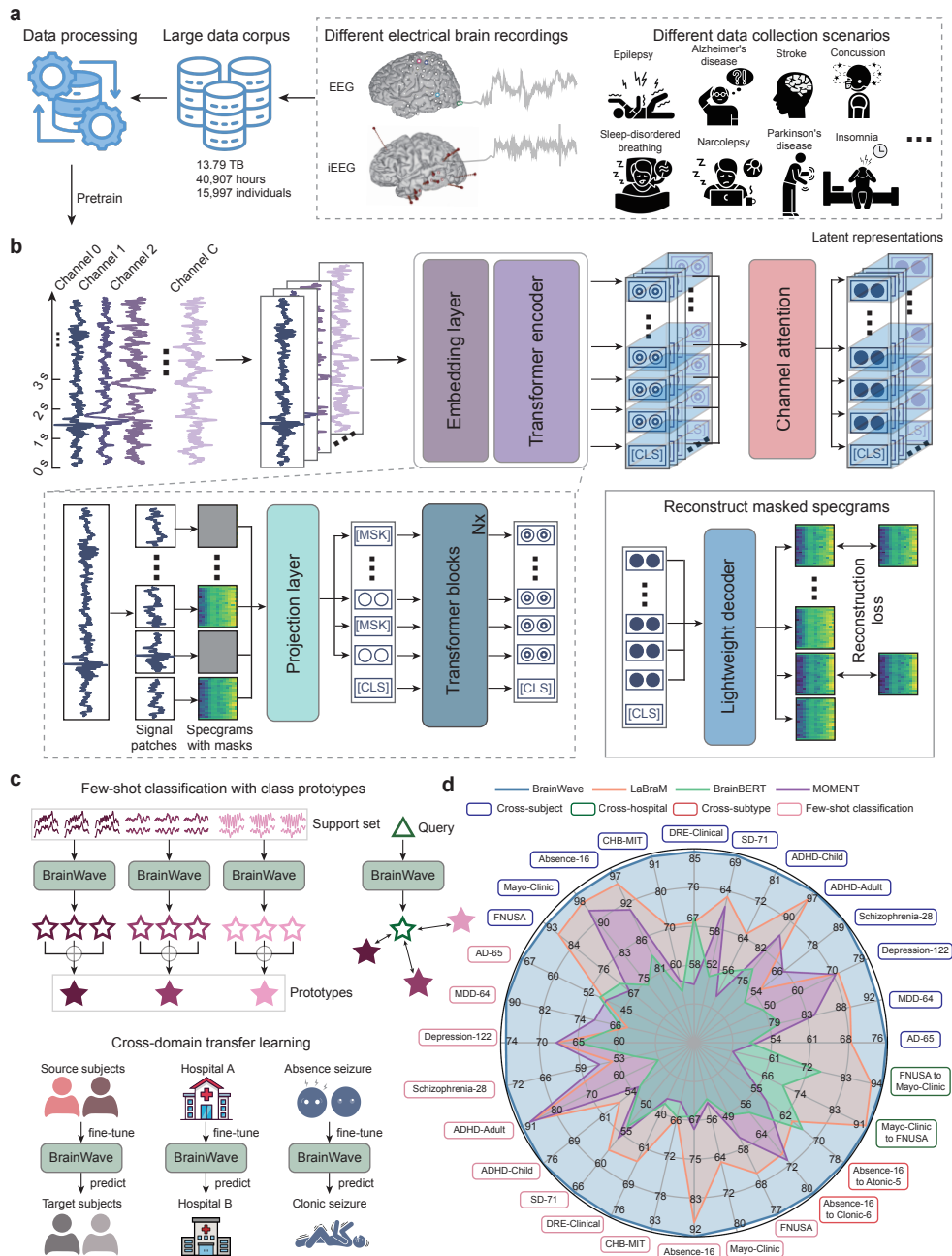


Fig. 1 Overview of BrainWave. **a**, Data curation for pretraining BrainWave. The pretraining corpus contains both invasive and non-invasive brain recordings collected from diverse healthcare scenarios. **b**, The pretraining pipeline of BrainWave. BrainWave is pretrained on more than 3 billion signal patches using a masked modeling strategy. **c**, The evaluation tasks consist of few-shot classification and cross-domain evaluation. We conduct few-shot classification with a prototypical network in which we directly compare the representations of the queries with class prototypes. We perform three different levels of cross-domain analysis: cross-subject, cross-hospital, and cross-subtype. **d**, The overall results of BrainWave compared to other pretrained models. BrainWave outperforms other models across all the 28 experiments, with significant improvement ($p < 0.001$) in 24 of them.

to successfully implement joint pretraining and validate its effectiveness. Overall, we demonstrated the potential of BrainWave to assist clinical diagnostics and decision support with strong scalability.

BrainWave not only exhibits potential for broad applications but also offers new insights for the development of foundation models based on brain signals. We will release BrainWave as an off-the-shelf and publicly available model, which will serve as a basis for others in their own tasks, facilitating diverse clinical applications and research for brain recordings.

2 Results

2.1 Cross-domain Disease Diagnosis and Detection

In real-world clinical applications, where the data of individuals to be diagnosed are usually unavailable during training, it is desirable for a model to be capable of making accurate predictions on unseen subjects. Thus, evaluating in a cross-subject setting is essential to accurately reflect a model’s performance and practical value in clinical scenarios. For each dataset, we split the subjects into n non-overlapping groups and employed n -fold cross validation to evaluate all models, ensuring that all subjects are included in the testing process. In each fold, we randomly selected a subject group from the training set for validation and repeated five runs. BrainWave was evaluated against competing methods on a total of 12 datasets, consisting of 10 publicly available datasets (Supplementary Tables 7-16) and 2 private datasets (Supplementary Tables 3 and 4). Model performance was reported using the area under the receiver operating curve (AUROC) and balanced accuracy (BACC). We calculated p values with the two-sided t -test between BrainWave and the most competitive comparison model for each task to check for significance.

Across all experiments, BrainWave consistently outperformed other methods with an average relative improvement of 12.61% in AUROC (Area Under the Receiver Operating Characteristic curve) and 16.44% in BACC (Balanced Accuracy) over each second-best performing model (Fig. 2a-l and Extended Data Fig. A1). In schizophrenia diagnosis (Fig. 2i; dataset Schizophrenia-28 [48]), BrainWave achieved an improvement of 37.44% and 41.59% compared to the best comparison model in terms of AUROC and BACC. In seizure detection (Fig. 2b; dataset CHB-MIT [49]), BrainWave demonstrated a 26.18% boost relative to the second best method. The strong performance of BrainWave on both ADHD-Adult [50] (Fig. 2j) and ADHD-Child [51] (Fig. 2k) indicated its robustness across age groups, owing to the broad age distribution in our pretraining corpus. In conclusion, BrainWave significantly surpassed other models ($p < 0.001$) on 11 out of the 12 datasets, demonstrating its superiority in disease diagnosis and detection.

The promising results of BrainWave on cross-subject evaluation motivated us to further explore its transfer capability across more divergent distributions. Thus, we attempted two more challenging experimental setups. Under these settings, we fine-tuned on one dataset and directly apply the model to another. These datasets are not only collected from different individuals but also from different hospitals and collection devices, or from patients with different disease subtypes. Unlike the traditional

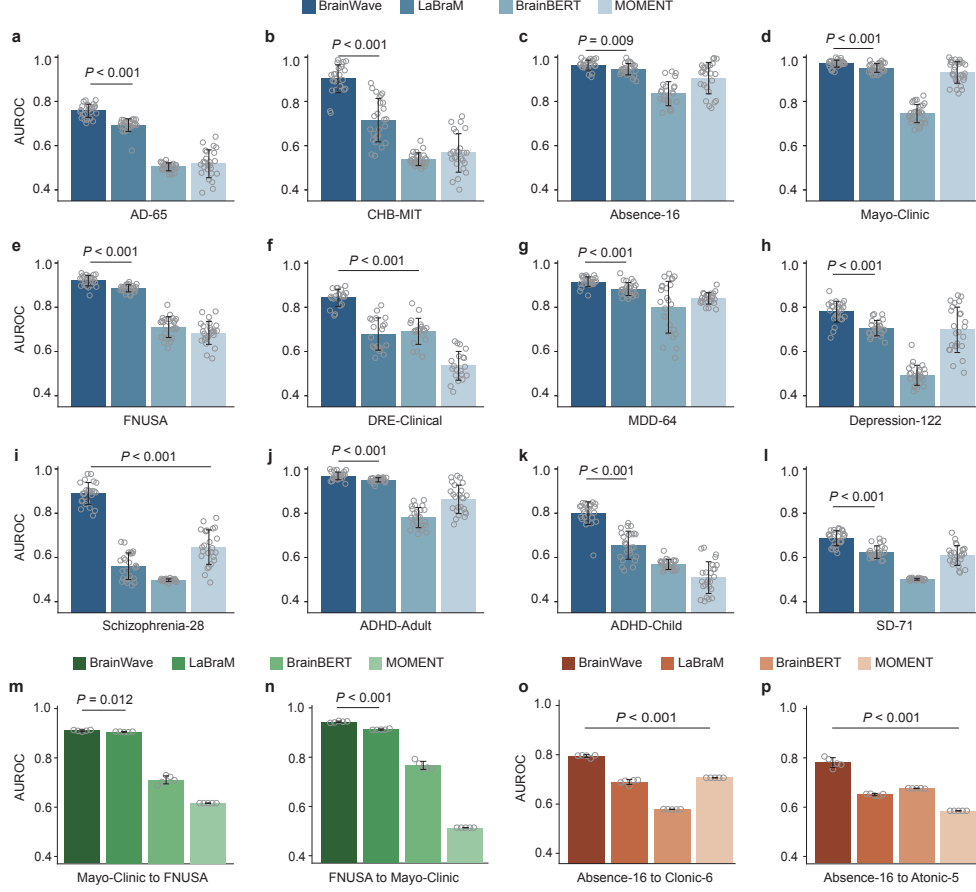


Fig. 2 Performance of cross-domain evaluation. **a-l**, Bar plots comparing the AUROC scores of BrainWave and competing models on cross-subject tasks. Each experiment is conducted with n -fold cross validation (n is the number of subject groups), where we repeat five runs for each fold. **m,n**, Bar plots comparing the AUROC scores of BrainWave and competing models on cross-hospital tasks. **o,p**, Bar plots comparing the AUROC scores of BrainWave and competing models on cross-subtype tasks. **m-p**, The source dataset is served as the training set and the target dataset is served as the evaluation set. In each experiment, we repeat five runs. **a-p**, Data are mean \pm SD. The listed p value indicates the significance for BrainWave outperforming the best comparison model, with the two-sided t -test.

paradigm where fine-tuning is dataset-specific, these settings allow the model to be seamlessly deployed across different datasets and even different but related tasks. The cross-hospital evaluation involved mutual transfer between two datasets, Mayo-Clinic and FNUSA [52], both collected from patients with drug resistant epilepsy but from different hospitals. The cross-subtype evaluation included three datasets, namely Absence-16, Clonic-6, and Atonic-5, collected from patients with different subtypes of seizures (absence seizure, clonic seizure, and atonic seizure), and we performed zero-shot transfer from Absence-16 to Clonic-6 and Atonic-5. BrainWave showed promising results and achieved the best performance in all cross evaluations (Fig. 2m-p and

Extended Data Fig. A2). For instance, BrainWave achieved an impressive AUROC of 93.82% in the zero-shot transfer from FNUSA to Mayo-Clinic (Fig. 2n). When transferring across different seizure subtypes (Fig. 2o,p), BrainWave exhibited average improvements of 13.90% and 13.49% in terms of AUROC and BACC, respectively, compared to the second-best model.

In summary, our experimental results indicated that BrainWave holds the potential to reduce labeling and training costs under similar scenarios, demonstrating promising applicability in real-world clinical tasks.

2.2 Few-shot Classification

In clinical practice, limited availability of labeled data sometimes poses challenges for fine-tuning models, which highlights the critical importance of learning sufficiently robust representations. Consequently, we performed few-shot classification, which is an evaluation scheme that studies the generalization capabilities of models on new tasks given a very limited number of labeled examples. We adopted a direct comparison strategy for classification by comparing the representations of the queries with prototype of each category (Fig. 1c). The process solely involved obtaining representations from the pretrained models and computing class prototypes, without any parameter updates or introduction of new parameters. The few-shot experiments were still conducted under the cross-subject setting and we employed n -fold cross validation, where in each fold we randomly chose labeled examples from the training set as the support set. We established two sizes for the support set, with 3 and 8 labeled examples per class (3-shot and 8-shot), respectively. Given that the performance can fluctuate depending on the support set, we repeated experiments over five runs in each fold. For comparison, we also trained an MLP (multilayer perceptron) from scratch with full-label supervision for each experiment.

We conducted few-shot experiments (Fig. 3a-l and Extended Data Fig. A3) on all datasets used in the cross-subject evaluation and found that BrainWave still maintained solid performance by achieving an average improvement of 21.21% in terms of AUROC compared to the second-best model. For instance, on Absence-16 (Fig. 3c) and ADHD-Adult (Fig. 3j), BrainWave achieved an AUROC over 90% (91.93% on Absence-16, 90.39% on ADHD-Adult) in 8-shot classification. On MDD-64 [53] (Fig. 3g), the performance of 8-shot learning even nearly matched that of full-label supervised fine-tuning (89.83% versus 91.50%). BrainWave not only outperformed other models by a large margin but also demonstrated greater robustness to the selection of the support set. Specifically, we calculated the average standard deviation across all few-shot experiments and found that the fluctuations in BrainWave’s performance are, on average, smaller than those of the second-best performing models (5.74% versus 6.06%). The poor performance of BrainBERT in few-shot classification may be due to its limitation in supporting only fixed-length inputs, which requires additional operations to accommodate varying input lengths, highlighting the importance of supporting variable-length inputs for a wide array of tasks.

When compared to the end-to-end trained MLP (Fig. 3m), BrainWave still achieved an average improvement of 25.79% and 26.60% in terms of AUROC and BACC, respectively. Surprisingly, we also observed that when comparing the 8-shot

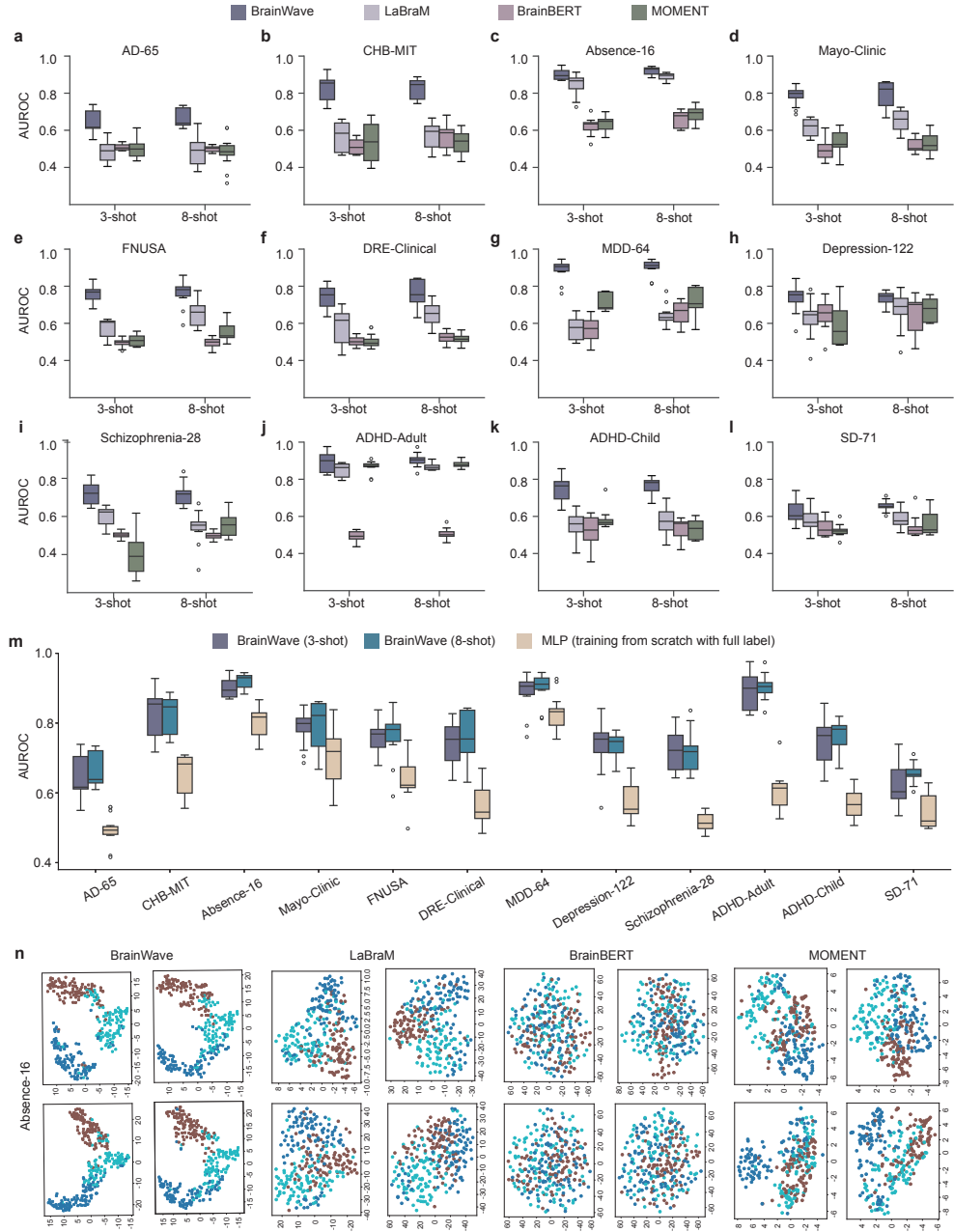


Fig. 3 Performance and analysis of few-shot classification. **a-l**, Box plots comparing the AUROC scores of BrainWave and competing models on few-shot classification. We conduct n -fold cross validation for each experiment and repeat five runs per fold. We perform 3-shot and 8-shot classification for each task. **m**, Box plots comparing the BACC scores of BrainWave on few-shot classification and end-to-end trained MLP with full-label supervision. **n**, t-SNE (t-distributed Stochastic Neighbor Embedding) plots of the pretrained representations on Absence-16 generated from BrainWave and other pretrained encoders. Each model contains four subplots, with each subplot generated by randomly sampling a portion of the original dataset.

performance of BrainWave with the full-label fine-tuning (i.e., with thousands or even tens of thousands of labeled examples) performance of other pretrained models, our model still outperforms on the majority of datasets (Extended Data Figs. A5 and A6). Specifically, BrainWave surpassed LaBraM, BrainBERT and MOMENT on 7, 12 and 11 out of 12 datasets, respectively. To better illustrate the results, we visualized the representations of the pretrained models, with different colored points representing different categories (Fig. 3n) and Extended Data Fig. A7). Even without fine-tuning, the representations generated by BrainWave are sufficiently discriminative and enable its outstanding performance in few-shot classification. Overall, our extensive evaluation of few-shot classification demonstrated the immense potential of BrainWave as a foundational model for electrical brain recordings that offers robust and off-the-shelf representations for various clinical applications.

2.3 Analysis of joint pretraining

To the best of our knowledge, BrainWave is the first foundational model that combines invasive and non-invasive neural data. We next examine the effectiveness of this joint pretraining strategy to determine whether it is more effective to pretrain a separate model for each recording type and apply it for corresponding downstream tasks with the same recording type, or to utilize a joint pretraining approach. To this end, we separately pretrained two model variants, namely BrainWave-EEG and BrainWave-iEEG, using EEG and iEEG data, respectively, while keeping the model and pretraining configurations (Supplementary Tables B19 and B18) identical to BrainWave. The numbers of patches for pretraining BrainWave-EEG and BrainWave-iEEG are relatively balanced (1.74 billion versus 1.42 billion). Subsequently, we conducted cross-domain evaluation and few-shot classification on both model variants, in which BrainWave-EEG was evaluated on EEG datasets and BrainWave-iEEG was evaluated on iEEG datasets.

Through a series of experiments, we observed that BrainWave outperformed the other two variants in almost all tasks and experimental settings (Fig. 4a-d and Extended Data and Figs. A8 and A10), except in experiment Absence-16 to Atonic-5 where BrainWave is slightly lower than BrainWave-EEG in terms of BACC (44.55% versus 47.23%). From the overall results, we discovered that the integration of iEEG during joint pretraining enhanced the performance on downstream tasks based on EEG data and vice versa, suggesting that BrainWave is able to capture fundamental insights about brain activities by combining two distinct types of signals. In comparison to the average improvement over two model variants (Fig. 4e), the improvement of the BrainWave over BrainWave-EEG was more significant than the improvement over BrainWave-iEEG (7.44% versus 2.58% on cross-domain evaluation and 8.13% versus 6.92% on few-shot classification in terms of AUROC). The phenomenon suggested that the boost in performance achieved by incorporating iEEG data in the pretraining was more pronounced, which might be attributed to the lower signal-to-noise ratio and higher accuracy of intracranial neural signals.

Given that joint pretraining leads to increase in performance, we further explored the underlying reasons by analyzing the representations learned by the models. First, we validated whether joint pretraining can learn more enriched information. For

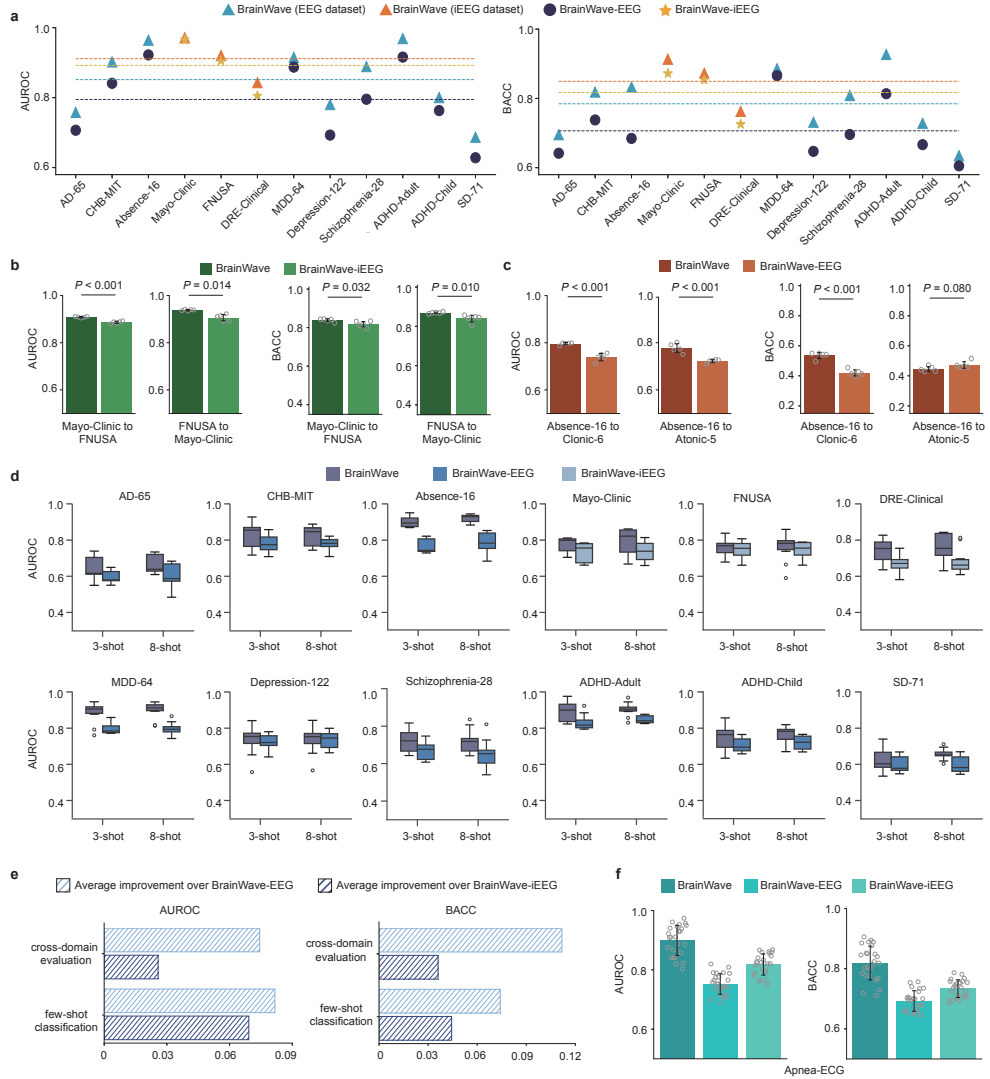


Fig. 4 Analysis of joint pretraining. **a**, Scatter plots comparing the AUROC and BACC scores of BrainWave, BrainWave-EEG and BrainWave-iEEG on cross-subject tasks. **b**, Bar plots comparing the AUROC and BACC scores of BrainWave and BrainWave-iEEG on cross-hospital tasks. **c**, Bar plots comparing the AUROC and BACC scores of BrainWave and BrainWave-EEG on cross-subtype tasks. **b,c**, The source dataset is served as the training set and the target dataset is served as the evaluation set. In each experiment, we repeat five runs. Data are mean \pm SD. The listed p value indicates the significance for BrainWave outperforming the best comparison model, with the two-sided t -test. **d**, Box plots comparing the AUROC scores of BrainWave, BrainWave-EEG and BrainWave-iEEG on few-shot classification. We perform 3-shot and 8-shot classification for each dataset. **e**, Average improvement of BrainWave over BrainWave-EEG and BrainWave-iEEG on cross-domain evaluation and few-shot classification. We first calculate the relative improvement for each experiment and then compute the average of them. **f**, Bar plots comparing the AUROC and BACC scores of BrainWave, BrainWave-EEG and BrainWave-iEEG on out-of-domain recording type evaluation. We collect a ECG dataset (Apnea-ECG) with a sleep apnea detection task. Data are mean \pm SD. **a,d,f**, Each experiment is conducted with n -fold cross validation (n is the number of subject groups), where we repeat five runs for each fold.

this purpose, we performed principal component analysis (PCA) to the pretrained representations, selecting principal components until 99% of the variance could be explained. We conducted analysis on 15 datasets and recorded the number of principal components k of each dataset. On 13 out of 14 datasets, BrainWave yielded a higher k value (Supplementary Tables B20 and B21), indicating that BrainWave demonstrated the ability to extract more enriched information from downstream datasets. Furthermore, we conducted an additional experiment by evaluating the performance of the BrainWave versus other variants on another type of biosignal, electrocardiogram (ECG), through which we aimed to verify if joint pretraining results in a stronger adaptability on new tasks due to the acquisition of more general patterns. The results (Fig. 4f) showed that BrainWave achieves an improvement of 9.90% and 19.48% in terms of AUROC over BrainWave-iEEG and BrainWave-EEG, respectively, demonstrating that joint pretraining enables better generalization to unseen data types. To summarize, BrainWave learned richer semantic information and more general patterns of the data than other model variants with only one type of data. This finding opens up possibilities for expanding signal types and developing more versatile foundational models for biosignals.

3 Discussion

We have introduced BrainWave, a brain signal foundation model that learns robust representations of electrical brain recordings for a broad range of clinical applications. To the best of our knowledge, BrainWave is the first model pretrained on a large-scale dataset composed of recordings from both invasive and non-invasive methods, which comprised more than 3 billion signal patches from approximately 16,000 individuals. We adopted a masked modeling strategy to pretrain BrainWave, in which the model learned to reconstruct the whole sequence given its partial observation. The architecture design allowed for brain recordings of varying lengths, sampling rates, and electrode counts, enhancing the flexibility of BrainWave for joint pretraining and deployment on iEEG and EEG data. In comprehensive experiments involving cross-domain evaluation and few-shot classification, we demonstrated the versatility of BrainWave across a wide array of healthcare tasks under different settings, which indicated the great potential of BrainWave assist clinical diagnostics and health condition detection.

Beyond its practical value, BrainWave also provides valuable insights for the development of foundation models based on brain signals. As the first study to adopt joint pretraining with EEG and iEEG data, we validated the effectiveness of this strategy. Through extensive evaluation, we observed a clear performance boost from joint pretraining compared to the model variants from control group. Furthermore, we revealed the reasons behind the performance enhancement attributed to joint training. Our work opens up new opportunities for leveraging similar techniques with other types of medical data, where efficient and scalable models are critical. In addition, this study provides a foundation for further exploration into joint pretraining across multiple medical data modalities. Future studies can build upon our findings to investigate

whether similar improvements can be achieved with other neural data types or even cross-domain data involving different physiological signals.

Despite the promising results, there is a wealth of potential for further development and advancement. Firstly, BrainWave is a unimodal model and cannot handle data from other modalities, such as magnetic resonance imaging (MRI), which can provide higher spatial resolution compared to electrical signals and is widely used in healthcare applications. Therefore, we hope to design a model framework going forward that is compatible with multiple modalities. Secondly, diverse medical scenarios collect various physiological signals, with diagnoses sometimes relying on multiple signal types. For instance, stroke diagnosis and rehabilitation often require the recording of EEG and EMG (Electromyography)[54]. To better serve more healthcare applications, the model should be capable of handling a wider range of biosignals. In this study, we only made preliminary attempts using ECG data, suggesting that there is still progress to be made before a comprehensive model capable of handling a diverse range of physiological signals is developed.

4 Methods

4.1 Technique details

Fig. 1b shows the overall architecture of BrainWave, which is composed of three main components: embedding layer, Transformer encoder and channel attention. This section aims to introduce the details of these components.

Embedding layer. The embedding layer of BrainWave projects the original signals into latent embeddings, in which each channel is operated independently. Given a single-channel brain recording, we first divided the signal into a series of consecutive non-overlapping 1-second patches $\mathbf{P}_i \in \mathbb{R}^{N \times P}$, where N is the number of patches, P is the number of timestamps in each 1-second patch, and i is the channel index. Then we calculated the time-frequency representations of each patch, in which we chose the spectrograms with Gaussian window. By keeping the ratio of the window size and the hop size to the patch length P constant, we can align recordings with different sampling rates onto spectrograms with consistent temporal and frequency resolutions. Specifically, we set the window size equal to $\frac{P}{4}$ and the hop size equal to $\frac{P}{8}$, and the resulting spectrograms are denoted as $\mathbf{S}_i \in \mathbb{R}^{N \times T \times F}$, where T is the length of the time axis and F is the length of the frequency axis. We convolved \mathbf{S}_i using 2D convolutional kernels to obtain the feature maps $\mathbf{M}_i \in \mathbb{R}^{N \times C_{\text{out}} \times T_{\text{out}} \times F_{\text{out}}}$, where C_{out} is the output channels and $T_{\text{out}} \times F_{\text{out}}$ is the size of the feature maps. Since our design ensured that data with different sampling rates have the same temporal and frequency resolution, the length of the time axis T_{out} in the resulting feature maps was the same (because the duration of all patches is 1 second), while the length of the frequency axis F_{out} varied. Therefore, we performed padding or truncation on the frequency axis to standardize the size of the feature maps. Then we flattened the standardized feature maps and projected them with a linear layer to derive the input embeddings $\mathbf{E}_i \in \mathbb{R}^{N \times D}$, where D is the hidden size.

Transformer encoder. The Transformer encoder is composed of stacked Transformer blocks with bidirectional self-attention, which captures the temporal relationship among the patches within a sequence. We first concatenated the input embeddings \mathbf{E}_i with a [CLS] token, then added a set of learnable positional embeddings $\mathbf{PE}_i \in \mathbb{R}^{(N+1) \times D}$ to obtain the input of the Transformer encoder. Like the embedding layer, the Transformer encoder encoded each channel independently and generated a set of outputs $\mathbf{O}_1, \mathbf{O}_2, \dots, \mathbf{O}_C$, where C is the number of channels. We derived the whole output $\mathbf{O} \in \mathbb{R}^{C \times (N+1) \times D}$ by concatenating the outputs together.

Channel attention. The channel attention module aims at capturing the correlation between different channels. Specifically, the input $\mathbf{O}^j \in \mathbb{R}^{C \times D}, j = 0, 1, \dots, N$ contained C different patches at the same time, which was then performed with a bidirectional self-attention operation. The output of the channel attention, denoted as $\mathbf{Z} \in \mathbb{R}^{C \times (N+1) \times D}$, served as the latent representation of BrainWave, where \mathbf{Z}^0 were sequence-level representations (representations of [CLS] tokens) and $\mathbf{Z}^1, \mathbf{Z}^2, \dots, \mathbf{Z}^N$ were patch-level representations.

4.2 Pretraining

Data curation. We curated large collections of unannotated electrical brain recordings for pretraining, totaling 13.79 TB data over a duration of 40,907 hours. The iEEG data were obtained from CCEP [55] and a private corpus collected by ourselves, comprising 10.63 TB of data. The recordings spanned a duration of 5231 hours and were collected from 91 subjects, ranging in age from 4 to 51 years. The sampling rate ranged from 1000 Hz to 4096 Hz, and the number of channels varied from 48 to 238. The EEG recordings consisted of CAP [56], HMC [57], Siena [58], SRM [59], TUEG [60], Schizophrenia-81, Sleep-EDF [61], Stroke-50 [62], PD-31 [63], IowaDataset, UNM-Dataset, AD-184 [64], and a private EEG corpus, with a total of 3.16 TB of data. The recording duration of the data reached 35,675.5 hours and involved 15,906 subjects, ranging in age from less than 1 year to over 90 years. The sampling rate ranged from 100 Hz to 1024 Hz, and the number of channels varied from 1 to 64.

The preprocessing of the pretraining data primarily involved channel selection, downsampling and filtering. Due to potential equipment issues during the data collection process, there might be invalid channels where no valid brain signals were captured. Therefore, we needed to perform channel selection, in which we visualized the recordings and manually selected the valid channels. We only downsampled signals with a sampling rate higher than 1000 Hz until they were below 1000 Hz, with the remaining signals preserved at their original sampling rates. Then, we applied a band-pass filter in the frequency range of 0.01 Hz to $\text{sfreq}/3$ Hz, where sfreq represents the sampling rate, and applied a notch filter at 50 Hz or 60 Hz to remove powerline noise.

Pretraining details. The main backbone of BrainWave is the RoBERTa [65] encoder architecture. The model had a hidden size of 768 and an intermediate size of 2048, with 10 layers and 16 attention heads. We applied absolute positional encoding with a maximum sequence length of 61 (60 signal patches along with a [CLS] token). We pretrained BrainWave on a total of 3,162,233,694 signal patches, including 1,739,447,411 EEG data patches and 1,422,786,283 iEEG data patches. BrainWave was trained using the AdamW optimizer [66], with $\beta_1 = 0.9$, $\beta_2 = 0.95$, $\text{eps} = 10^{-5}$.

For the learning rate scheduling, we utilized a linear warmup of 1000 steps to reach a peak learning rate of 1.0×10^{-5} , followed by a cosine decay of 30,000 steps to decay the final learning rate to 0. The total training steps of BrainWave was 16,600. We employed gradient accumulation during pretraining, where we accumulated gradients for 16 times of forward and backward before performing a parameter update. The training process was conducted on $4 \times A100$ GPUs with a global batch size of 2,560,000 (patches) and the entire process took 100 hours.

4.3 Downstream evaluation

Competing methods. We compared BrainWave to 3 publicly available models: LaBraM [44], BrainBERT [46] and MOMENT [47]. LaBraM is an open-weight model pretrained on more than 2500 hours of EEG data. It tokenized the EEG into discrete tokens by training a neural tokenizer, and was pretrained with symmetric masked modeling. BrainBERT is a reusable, off-the-shelf, subject-agnostic, and electrode-agnostic model that provides embeddings for intracranial recordings. It was pretrained on 43.7 hours of iEEG data recorded from 10 subjects. During pretraining, it masked multiple continuous bands of random frequencies and time intervals in the time-frequency representations. MOMENT is a family of open-source foundation models for general-purpose time series analysis. It was pretrained on a large collection of publicly available datasets from 13 different domains, which included 20.085 GB (≈ 0.02 TB) worth of 13 million unique time series and 1.23 billion timestamps (0.15 billion patches). MOMENT also adopted a masked modeling strategy by masking and reconstructing the original time series.

Evaluation datasets. The evaluation benchmark comprised 15 distinct datasets, which contain 7 different healthcare scenarios.

Alzheimer’s disease: AD-65 [67] contains the EEG resting state-closed eyes recordings from 88 subjects in total (44 males, ages 53–79; and 44 females, ages 44–79). For the participants, 36 were diagnosed with Alzheimer’s disease (AD group), 23 were diagnosed with Frontotemporal Dementia (FTD group) and 29 were healthy subjects (CN group). We randomly split the subjects from AD group and CN group into 5 groups. The data comprised 19 channels with a sampling rate of 250 Hz. After processing, we obtained a total of 5349 samples and each sample contains a 10-second data segment.

Epilepsy: The CHB-MIT [49, 68] database consists of EEG recordings from 22 pediatric subjects (5 males, ages 3–22; and 17 females, ages 1.5–19) with intractable seizures. We randomly split the subjects into 5 groups. The data comprised 23 channels with a sampling rate of 256 Hz. We split the data into 10-second segments and obtained 4148 samples in total. Absence-16, Clonic-6 and Atonic-5 are 3 private datasets that were collected from patients with absence seizures, clonic seizures and atonic seizures, respectively. The annotations were divided into three categories: epileptic waveforms, normal waveforms, and Interictal epileptiform discharge (IED). The recordings comprised 19 channels with a sampling rate of 256 Hz. After processing the data into 4-second segments, we obtained a total of 8016 samples from Absence-16, 2426 samples from Clonic-6, and 1587 samples from Atonic-5. We randomly divided the 16 patients in Absence-16 into 5 groups. The Mayo-Clinic [52] data were collected between 1 AM and 3 AM from 25 patients with drug resistant epilepsy

(DRE) undergoing evaluation for epilepsy surgery. The FNUSA [52] dataset is made up of iEEG data collected in awake resting state from 14 patients diagnosed with DRE. These patients underwent a standard pre-surgical monitoring for localization of seizure onset zone (SOZ), a standard procedure for epilepsy surgery. We split Mayo-Clinic and FNUSA into 6 and 5 subject groups, respectively. Both Mayo-Clinic and FNUSA were segmented into 3-second data clips and downsampled to 1000 Hz. In order to locate the SOZ, annotations were made for each channel. We preserved the data segments annotated with physiological activity, pathological (epileptic) activity and artifacts. In total, Mayo-Clinic contained 113,260 samples and FNUSA contained 179,629 samples. DRE-Clinical is a private dataset that contains the iEEG recordings from 8 patients with DRE. The annotation was also channel-wise for SOZ localization. We split the patients into 4 groups, with two individuals in each group. The recordings were segmented into 20-second data clips and we obtained 229,932 samples in total.

Depression: MDD-64 [53] contains EEG recordings from 64 subjects with 34 of them diagnosed with Major Depressive Disorder (MDD). We randomly split the subjects into 5 groups. The data comprised 19 channels with a sampling rate of 256 Hz. We split the data into 10-second segments and obtained 7309 samples in total. Depression-122 [69] consists of resting EEG data with 122 college-age participants (47 males, ages 18–24; 74 females, ages 18–23; and 1 unknown) with their scores in Beck Depression Inventory (BDI). According to [70], participants with BDI scores > 13 were considered depressed. Healthy controls had stable low BDI scores (< 7) and no self-reported history or symptoms of anxiety disorder. The data comprised 64 channels with a sampling rate of 500 Hz. We split the data into 10-second segments and obtained 5836 samples in total.

Schizophrenia: Schizophrenia-28 [48] comprises 14 patients with paranoid schizophrenia and 14 healthy controls. Data were acquired with the sampling frequency of 250 Hz using the standard 10-20 EEG montage with 19 EEG channels. We randomly split the subjects into 5 groups. For the EEG recordings, we split the data into 10-second segments and obtained 5744 samples.

Attention deficit hyperactivity disorder (ADHD): ADHD-Adult [50] was collected from 79 participants, including 42 healthy adults and 37 adults with ADHD (age 20–68 years; male/female: 56/23). The dataset contained 256 Hz EEG signals recorded from five channels, including O1, F3, F4, Cz, and Fz, with each subject recorded with two channels. The subjects were randomly split into 5 groups. We split the data into 5-second segments and obtained 5056 samples in total. ADHD-Child [51] contains EEG data collected from 121 children (ages 7–12), including 61 with ADHD and 60 healthy controls. The EEG recordings were performed based on 10-20 standard by 19 channels at 128 Hz sampling frequency. We randomly split the subjects into 5 groups. After processing, we obtained a total of 3322 samples and each sample contains a 5-second data segment.

Sleep Deprivation: SD-71 [71] provides resting-state EEG data from 71 participants who underwent two experiments involving normal sleep and sleep deprivation. We randomly split the subjects into 5 groups. The data comprised 61 channels with a sampling rate of 500 Hz. We split the data into 5-second segments and obtained 13,700 samples in total.

Sleep Apnea: Apnea-ECG [72] is an annotated database with 70 nighttime ECG recordings. Each recording included a continuous digitized ECG signal with a sampling rate of 100 Hz. We divided the recordings into 5 groups, split the data into 60-second segments, and obtained 34,271 samples in total.

Cross-subject evaluation. The cross-subject evaluation involved experiments on 12 datasets: AD-65 (Alzheimer’s disease diagnosis), CHB-MIT (seizure detection), Absence-16 (seizure detection), Mayo-Clinic (seizure detection and SOZ localization), FNUSA (seizure detection and SOZ localization), DRE-Clinical (seizure detection and SOZ localization), MDD-64 (MDD diagnosis), Depression-122 (depression diagnosis), Schizophrenia-28 (schizophrenia diagnosis), ADHD-Adult (ADHD diagnosis), ADHD-child (ADHD diagnosis) and SD-71 (sleep deprivation detection). We used the AdamW optimizer for fine-tuning, with $\beta_1 = 0.9$, $\beta_2 = 0.95$, $eps = 10^{-5}$. For all the models, we fine-tuned the pretrained encoder and the classification head with a learning rate of 1×10^{-5} and 1×10^{-4} . The models were trained for up to 30 epochs, and then the best-performing models on the validation set were selected for testing.

Cross-hospital and cross-subtype evaluation. The cross-hospital evaluation involved Mayo-Clinic and FNUSA, and the cross-subtype evaluation involved Absence-16, Clonic-6, and Atonic-5. In the experiments, we fine-tune the models on the source dataset with a fixed number of epochs and directly evaluated on the target dataset. We used the AdamW optimizer, with $\beta_1 = 0.9$, $\beta_2 = 0.95$, $eps = 10^{-5}$. We fine-tuned the pretrained encoder and the classification head for 5 epochs with a learning rate of 1×10^{-5} and 1×10^{-4} .

Few-shot classification. The datasets used for few-shot classification were identical to those used for cross-subject evaluation. We classified the queries by comparing with prototypes. Specifically, in K -shot, M -class classification, given the representations of the support set $\{\mathbf{u}_i^j | i = 1, 2, \dots, K; j = 1, 2, \dots, M\}$, we obtained the prototypes for each class as the mean of the examples: $\{\mathbf{v}^j = \frac{1}{K} \sum_{i=1}^K \mathbf{u}_i^j | j = 1, 2, \dots, M\}$. Given the representation of a query $\mathbf{z} \in \mathbb{R}^{C \times D}$, where C is the number of channels and D is the hidden size, we calculated the channel-wise cosine similarities between the query representation and prototypes: $\{\text{sim}^j = \cos(\mathbf{z}, \mathbf{v}^j) \in \mathbb{R}^C | j = 1, 2, \dots, M\}$. The scores of the query were the mean of channel-wise similarities and we chose the class with the highest score as the prediction: $y_{\text{pred}} = \text{argmax}([s^1, s^2, \dots, s^M])$, where $s^j = \sum_{c=1}^C \text{sim}_c^j$.

References

- [1] Barborica, A., Mindruta, I., López-Madróna, V.J., Alario, F.-X., Trébuchon, A., Donos, C., Oane, I., Pistol, C., Mihai, F., Bénar, C.G.: Studying memory processes at different levels with simultaneous depth and surface eeg recordings. *Frontiers in Human Neuroscience* **17** (2023) <https://doi.org/10.3389/fnhum.2023.1154038>
- [2] Jiang, S., Patel, D.C., Kim, J., *et al.*: Spatially expandable fiber-based probes as a multifunctional deep brain interface. *Nature Communications* **11**(1), 6115 (2020) <https://doi.org/10.1038/s41467-020-19946-9>

- [3] Engel, A.K., Moll, C.K., Fried, I., Ojemann, G.A.: Invasive recordings from the human brain: clinical insights and beyond. *Nature Reviews Neuroscience* **6**(1), 35–47 (2005)
- [4] Pesaran, B., Vinck, M., Einevoll, G.T., Sirota, A., Fries, P., Siegel, M., Truccolo, W., Schroeder, C.E., Srinivasan, R.: Investigating large-scale brain dynamics using field potential recordings: analysis and interpretation. *Nature neuroscience* **21**(7), 903–919 (2018)
- [5] Urai, A.E., Doiron, B., Leifer, A.M., Churchland, A.K.: Large-scale neural recordings call for new insights to link brain and behavior. *Nature neuroscience* **25**(1), 11–19 (2022)
- [6] Khodagholy, D., Gelinias, J.N., Thesen, T., Doyle, W., Devinsky, O., Malliaras, G.G., Buzsáki, G.: Neurogrid: recording action potentials from the surface of the brain. *Nature neuroscience* **18**(2), 310–315 (2015)
- [7] Horejs, C.M.: Long-term recording of electrical activity in brain organoids. *Nature Reviews Bioengineering* **2**, 200 (2024) <https://doi.org/10.1038/s44222-024-00164-7>
- [8] Shih, J.J., Krusienski, D.J., Wolpaw, J.R.: Brain-computer interfaces in medicine. *Mayo Clinic Proceedings* **87**(3), 268–279 (2012) <https://doi.org/10.1016/j.mayocp.2011.12.008>
- [9] Feigin, V.L., Vos, T., Nichols, E., al.: The global burden of neurological disorders: translating evidence into policy. *Lancet Neurology* **19**(3), 255–265 (2020) [https://doi.org/10.1016/S1474-4422\(19\)30411-9](https://doi.org/10.1016/S1474-4422(19)30411-9)
- [10] Soufneyestani, M., Dowling, D., Khan, A.: Electroencephalography (eeg) technology applications and available devices. *Applied Sciences* **10**(21) (2020) <https://doi.org/10.3390/app10217453>
- [11] Vărbu, K., Muhammad, N., Muhammad, Y.: Past, present, and future of EEG-Based BCI applications. *Sensors (Basel)* **22**(9), 3331 (2022) <https://doi.org/10.3390/s22093331> . Published 2022 Apr 26
- [12] Jadhav, C., Kamble, P., Mundewadi, S., *et al.*: Clinical applications of EEG as an excellent tool for event related potentials in psychiatric and neurotic disorders. *International Journal of Physiology, Pathophysiology and Pharmacology* **14**(2), 73–83 (2022). Published 2022 Apr 15
- [13] Silva, C., Tedesco, S., O’Flynn, B.: Eeg datasets for healthcare: A scoping review. *IEEE Access* **PP**, 1–1 (2024) <https://doi.org/10.1109/ACCESS.2024.3376254>
- [14] Amer, N.S., Belhaouari, S.B.: Eeg signal processing for medical diagnosis, healthcare, and monitoring: A comprehensive review. *IEEE Access* **11**, 143116–143142

(2023) <https://doi.org/10.1109/ACCESS.2023.3341419>

- [15] Yamada, L., Oskotsky, T., Nuyujukian, P., Center, S.C.E., Center, S.P.E.: A scalable platform for acquisition of high-fidelity human intracranial EEG with minimal clinical burden. *PLOS ONE* **19**(6), 0305009 (2024) <https://doi.org/10.1371/journal.pone.0305009> . Published 2024 Jun 13
- [16] Dasgupta, D., Miserocchi, A., McEvoy, A.W., Duncan, J.S.: Previous, current, and future stereotactic eeg techniques for localising epileptic foci. *Expert Review of Medical Devices* **19**, 571–580 (2022)
- [17] Parvizi, J., Kastner, S.: Promises and limitations of human intracranial electroencephalography. *Nature Neuroscience* **21**(4), 474–483 (2018) <https://doi.org/10.1038/s41593-018-0108-2>
- [18] Lachaux, J.P., Rudrauf, D., Kahane, P.: Intracranial eeg and human brain mapping. *Journal of Physiology-Paris* **97**(4-6), 613–628 (2003)
- [19] Meskó, B.: Data annotators are the unsung heroes of medicine’s artificial intelligence revolution. *Journal of Medical Artificial Intelligence* **3**(0) (2019)
- [20] Pascual, D., Aminifar, A., Atienza, D.: A self-learning methodology for epileptic seizure detection with minimally-supervised edge labeling. In: 2019 Design, Automation & Test in Europe Conference & Exhibition (DATE), pp. 764–769 (2019). <https://doi.org/10.23919/DATE.2019.8714995>
- [21] Zhao, X., Zhao, Q., Tanaka, T., al.: Classification of the epileptic seizure onset zone based on partial annotation. *Cognitive Neurodynamics* **17**(3), 703–713 (2023) <https://doi.org/10.1007/s11571-022-09857-4>
- [22] Friedman, D.E., Hirsch, L.J.: How long does it take to make an accurate diagnosis in an epilepsy monitoring unit? *Journal of Clinical Neurophysiology* **26**(4), 213–217 (2009) <https://doi.org/10.1097/WNP.0b013e3181b2f2da>
- [23] Brown, T.T.: Individual differences in human brain development. *Wiley Interdisciplinary Reviews: Cognitive Science* **8**(1-2), 1389 (2017) <https://doi.org/10.1002/wcs.1389>
- [24] Yuan, Z., Zhang, D., Yang, Y., Chen, J., Li, Y.: PPI: Pretraining brain signal model for patient-independent seizure detection. In: Thirty-seventh Conference on Neural Information Processing Systems (2023)
- [25] Clemente-Suárez, V.J., Redondo-Flórez, L., Beltrán-Velasco, A.I., Ramos-Campo, D.J., Belinchón-deMiguel, P., Martínez-Guardado, I., Dalamitros, A.A., Yáñez-Sepúlveda, R., Martín-Rodríguez, A., Tornero-Aguilera, J.F.: Mitochondria and brain disease: a comprehensive review of pathological mechanisms and therapeutic opportunities. *Biomedicines* **11**(9), 2488 (2023)

- [26] McEwen, B.S., Bowles, N.P., Gray, J.D., Hill, M.N., Hunter, R.G., Karatsoreos, I.N., Nasca, C.: Mechanisms of stress in the brain. *Nature neuroscience* **18**(10), 1353–1363 (2015)
- [27] Delgado-Morales, R., Agís-Balboa, R.C., Esteller, M., Berdasco, M.: Epigenetic mechanisms during ageing and neurogenesis as novel therapeutic avenues in human brain disorders. *Clinical epigenetics* **9**, 1–18 (2017)
- [28] Gaiteri, C., Ding, Y., French, B., Tseng, G.C., Sibille, E.: Beyond modules and hubs: the potential of gene coexpression networks for investigating molecular mechanisms of complex brain disorders. *Genes, brain and behavior* **13**(1), 13–24 (2014)
- [29] Yang, S., Zhang, Z., Chen, H., Meng, Y., Li, J., Li, Z., Xu, Q., Zhang, Q., Fan, Y.-S., Lu, G., *et al.*: Temporal variability profiling of the default mode across epilepsy subtypes. *Epilepsia* **62**(1), 61–73 (2021)
- [30] Guo, J., Li, H., Sun, X., Qi, L., Qiao, H., Pan, Y., Xiang, J., Ji, R.: Detecting high frequency oscillations for stereoelectroencephalography in epilepsy via hypergraph learning. *IEEE Transactions on Neural Systems and Rehabilitation Engineering* **29**, 587–596 (2021)
- [31] Wang, Y., Yang, Y., Cao, G., Guo, J., Wei, P., Feng, T., Dai, Y., Huang, J., Kang, G., Zhao, G.: Seeg-net: An explainable and deep learning-based cross-subject pathological activity detection method for drug-resistant epilepsy. *Computers in Biology and Medicine* **148**, 105703 (2022) <https://doi.org/10.1016/j.combiomed.2022.105703>
- [32] Chen, J., Yang, Y., Yu, T., Fan, Y., Mo, X., Yang, C.: Brainnet: Epileptic wave detection from seeg with hierarchical graph diffusion learning. In: *Proceedings of the 28th ACM SIGKDD Conference on Knowledge Discovery and Data Mining*, pp. 2741–2751 (2022)
- [33] Bagherzadeh, S., Shahabi, M.S., Shalhaf, A.: Detection of schizophrenia using hybrid of deep learning and brain effective connectivity image from electroencephalogram signal. *Computers in Biology and Medicine* **146**, 105570 (2022) <https://doi.org/10.1016/j.combiomed.2022.105570>
- [34] Sahu, G., Karnati, M., Gupta, A., Seal, A.: Scz-scan: An automated schizophrenia detection system from electroencephalogram signals. *Biomedical Signal Processing and Control* **86**, 105206 (2023) <https://doi.org/10.1016/j.bspc.2023.105206>
- [35] Miltiadous, A., Gionanidis, E., Tzimourta, K.D., Giannakeas, N., Tzallas, A.T.: Dice-net: A novel convolution-transformer architecture for alzheimer detection in eeg signals. *IEEE Access* **11**, 71840–71858 (2023) <https://doi.org/10.1109/ACCESS.2023.3294618>

- [36] Vicchietti, M.L., Ramos, F.M., Betting, L.E., *et al.*: Computational methods of EEG signals analysis for Alzheimer’s disease classification. *Scientific Reports* **13**, 8184 (2023) <https://doi.org/10.1038/s41598-023-32664-8>
- [37] Sun, X., Xu, Y., Zhao, Y., Zheng, X., Zheng, Y., Cui, L.: Multi-granularity graph convolution network for major depressive disorder recognition. *IEEE Transactions on Neural Systems and Rehabilitation Engineering* **32**, 559–569 (2024) <https://doi.org/10.1109/TNSRE.2023.3311458>
- [38] Zhou, Y., Chia, M.A., Wagner, S.K., *et al.*: A foundation model for generalizable disease detection from retinal images. *Nature* **622**, 156–163 (2023) <https://doi.org/10.1038/s41586-023-06555-x>
- [39] Chen, R.J., Ding, T., Lu, M.Y., *et al.*: Towards a general-purpose foundation model for computational pathology. *Nature Medicine* **30**, 850–862 (2024) <https://doi.org/10.1038/s41591-024-02857-3>
- [40] Xu, H., Usuyama, N., Bagga, J., *et al.*: A whole-slide foundation model for digital pathology from real-world data. *Nature* **630**, 181–188 (2024) <https://doi.org/10.1038/s41586-024-07441-w>
- [41] Pai, S., Bontempi, D., Hadzic, I., *et al.*: Foundation model for cancer imaging biomarkers. *Nature Machine Intelligence* **6**, 354–367 (2024) <https://doi.org/10.1038/s42256-024-00807-9>
- [42] Zhang, K., Zhou, R., Adhikarla, E., *et al.*: A generalist vision–language foundation model for diverse biomedical tasks. *Nature Medicine* (2024) <https://doi.org/10.1038/s41591-024-03185-2>
- [43] Hao, M., Gong, J., Zeng, X., *et al.*: Large-scale foundation model on single-cell transcriptomics. *Nature Methods* **21**, 1481–1491 (2024) <https://doi.org/10.1038/s41592-024-02305-7>
- [44] Jiang, W., Zhao, L., Lu, B.-l.: Large brain model for learning generic representations with tremendous EEG data in BCI. In: *The Twelfth International Conference on Learning Representations* (2024)
- [45] Zhang, D., Yuan, Z., Yang, Y., Chen, J., Wang, J., Li, Y.: Brant: Foundation model for intracranial neural signal. In: *Thirty-seventh Conference on Neural Information Processing Systems* (2023)
- [46] Wang, C., Subramaniam, V., Yaari, A.U., Kreiman, G., Katz, B., Cases, I., Barbu, A.: BrainBERT: Self-supervised representation learning for intracranial recordings. In: *The Eleventh International Conference on Learning Representations* (2023)
- [47] Goswami, M., Szafer, K., Choudhry, A., Cai, Y., Li, S., Dubrawski, A.:

- MOMENT: A family of open time-series foundation models. In: Forty-first International Conference on Machine Learning (2024)
- [48] Olejarczyk, E., Jernajczyk, W.: EEG in Schizophrenia. <https://doi.org/10.18150/repod.0107441>
- [49] Guttag, J.: CHB-MIT Scalp EEG Database. PhysioNet (2010). <https://doi.org/10.13026/C2K01R>
- [50] Sadeghi Bajestani, G., Abedian, S., Makhlooghi, F., Raoufitabar, M., Saeedi, H.: A Dataset of EEG Signals from Adults with ADHD and Healthy Controls: Resting State, Cognitive function, and Sound Listening Paradigm. Mendeley Data (2023). <https://doi.org/10.17632/6k4g25fhzg.1>
- [51] Motie Nasrabadi, A., Allahverdy, A., Samavati, M., Mohammadi, M.R.: EEG Data for ADHD / Control Children. <https://doi.org/10.21227/rzfh-zn36>
- [52] Nejedly, P., Kremen, V., Sladky, V., Cimbalko, J., Klimes, P., Plesinger, F., Mivalt, F., Travnicek, V., Viscor, I., Pail, M., et al.: Multicenter intracranial eeg dataset for classification of graphoelements and artifactual signals. Scientific data **7** (2020)
- [53] Mumtaz, W.: MDD Patients and Healthy Controls EEG Data (New). figshare. Dataset (2016). <https://doi.org/10.6084/m9.figshare.4244171.v2> . <https://doi.org/10.6084/m9.figshare.4244171.v2>
- [54] Jo, S., Jung, J.H., Yang, M.J., Lee, Y., Jang, S.J., Feng, J., Heo, S.H., Kim, J., Shin, J.H., Jeong, J., Park, H.S.: Eeg-emg hybrid real-time classification of hand grasp and release movements intention in chronic stroke patients. In: 2022 IEEE International Conference on Rehabilitation Robotics (ICORR), pp. 1–6 (2022). <https://doi.org/10.1109/ICORR55369.2022.9896592>
- [55] Blooijs, D., Boom, M.A., Aar, J.F., Huiskamp, G.J.M., Castegnaro, G., Demuru, M., Zweiphenning, W.J.E.M., Eijdsden, P., Miller, K.J., Leijten, F.S.S., Hermes, D.: "CCEP ECoG Dataset Across Age 4-51". <https://doi.org/10.18112/openneuro.ds004080.v1.2.4>
- [56] Terzano, M.G., Parrino, L., Sherieri, A., Chervin, R., Chokroverty, S., Guilleminault, C., Hirshkowitz, M., Mahowald, M., Moldofsky, H., Rosa, A., Thomas, R., Walters, A.: Atlas, rules, and recording techniques for the scoring of cyclic alternating pattern (cap) in human sleep. Sleep Medicine **2**(6), 537–553 (2001) [https://doi.org/10.1016/s1389-9457\(01\)00149-6](https://doi.org/10.1016/s1389-9457(01)00149-6) . Erratum in: Sleep Med. 2002 Mar;3(2):185
- [57] Alvarez-Estevéz, D., Rijsman, R.M.: Inter-database validation of a deep learning approach for automatic sleep scoring. PLoS ONE **16**(8), 0256111 (2021) <https://doi.org/10.1371/journal.pone.0256111>

- [58] Detti, P., Vatti, G., Lara, G.: Eeg synchronization analysis for seizure prediction: A study on data of noninvasive recordings. *Processes* **8**(7) (2020) <https://doi.org/10.3390/pr8070846>
- [59] Hatlestad-Hall, C., Rygvold, T.W., Andersson, S.: "SRM Resting-state EEG". <https://doi.org/10.18112/openneuro.ds003775.v1.2.1>
- [60] Harati, A., Lopez, S., Obeid, I., Picone, J., Jacobson, M., Tobochnik, S.: The tuh eeg corpus: A big data resource for automated eeg interpretation. In: 2014 IEEE Signal Processing in Medicine and Biology Symposium (SPMB) (2014)
- [61] Kemp, B., Zwinderman, A.H., Tuk, B., Kamphuisen, H.A.C., Obery, J.J.L.: Analysis of a sleep-dependent neuronal feedback loop: the slow-wave microcontinuity of the eeg. *IEEE Transactions on Biomedical Engineering* **47**(9), 1185–1194 (2000) <https://doi.org/10.1109/10.867928>
- [62] Liu, H., Lv, X.: EEG datasets of stroke patients (2022) <https://doi.org/10.6084/m9.figshare.21679035.v5>
- [63] Rockhill, A.P., Jackson, N., George, J., Aron, A., Swann, N.C.: "UC San Diego Resting State EEG Data from Patients with Parkinson's Disease". <https://doi.org/10.18112/openneuro.ds002778.v1.0.5>
- [64] Vicchietti, M.L., Ramos, F.M., Betting, L.E., Campanharo, A.S.: Computational methods of eeg signals analysis for alzheimer's disease classification. *Scientific Reports* **13**(1), 8184 (2023)
- [65] Liu, Y., Ott, M., Goyal, N., Du, J., Joshi, M., Chen, D., Levy, O., Lewis, M., Zettlemoyer, L., Stoyanov, V.: RoBERTa: A Robustly Optimized BERT Pretraining Approach (2019). <https://arxiv.org/abs/1907.11692>
- [66] Loshchilov, I., Hutter, F.: Decoupled Weight Decay Regularization (2019). <https://arxiv.org/abs/1711.05101>
- [67] Miltiadous, A., Tzimourta, K.D., Afrantou, T., Ioannidis, P., Grigoriadis, N., Tsalikakis, D.G., Angelidis, P., Tsipouras, M.G., Glavas, E., Giannakeas, N., Tzallas, A.T.: "A Dataset of 88 EEG Recordings From: Alzheimer's Disease, Frontotemporal Dementia and Healthy Subjects". <https://doi.org/10.18112/openneuro.ds004504.v1.0.2>
- [68] Shoeb, A.H.: Application of machine learning to epileptic seizure onset detection and treatment. PhD thesis, Massachusetts Institute of Technology (2009)
- [69] jcavanagh@unm.edu, J.F.C.: "EEG: Depression Rest". <https://doi.org/10.18112/openneuro.ds003478.v1.1.0>
- [70] Chang, J., Choi, Y.: Depression diagnosis based on electroencephalography power

ratios. *Brain and Behavior* **13**(8), 3173 (2023)

- [71] Xiang, C., Fan, X., Bai, D., Lv, K., Lei, X.: "A Resting-state EEG Dataset for Sleep Deprivation". <https://doi.org/10.18112/openneuro.ds004902.v1.0.5>
- [72] Penzel, T., Moody, G.B., Mark, R.G., Goldberger, A.L., Peter, J.H.: The apnea-ecg database. In: *Computers in Cardiology 2000*. Vol.27 (Cat. 00CH37163), pp. 255–258 (2000). <https://doi.org/10.1109/CIC.2000.898505>

Appendix A Extended Data

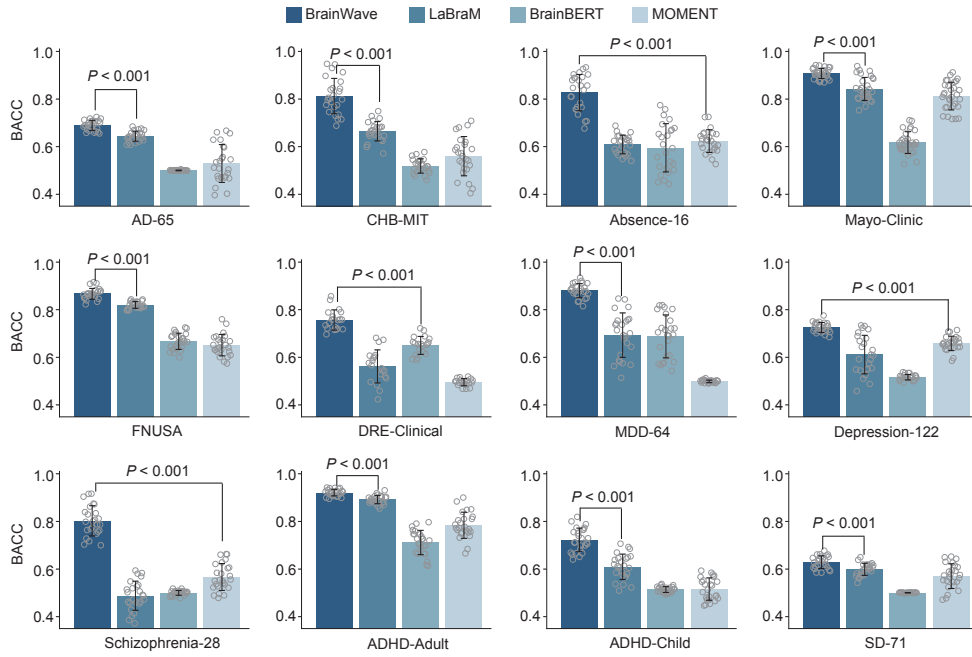


Fig. A1 Performance of cross-subject tasks. Bar plots comparing the BACC scores of BrainWave and competing models on cross-subject tasks. Data are mean \pm SD. Each experiment is conducted with n -fold cross validation (n is the number of subject groups), where we repeat five runs for each fold. The listed p value indicates the significance for BrainWave outperforming the best comparison model, with the two-sided t -test.

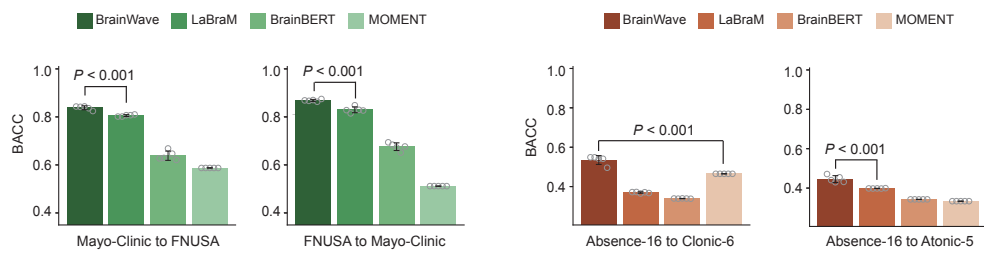


Fig. A2 Performance of cross-hospital and cross-subtype tasks. **a**, Bar plots comparing the BACC scores of BrainWave and competing models on cross-hospital tasks. **b**, Bar plots comparing the BACC scores of BrainWave and competing models on cross-subtype tasks. Data are mean \pm SD. Each experiment is repeated five runs. The listed p value indicates the significance for BrainWave outperforming the best comparison model, with the two-sided t -test.

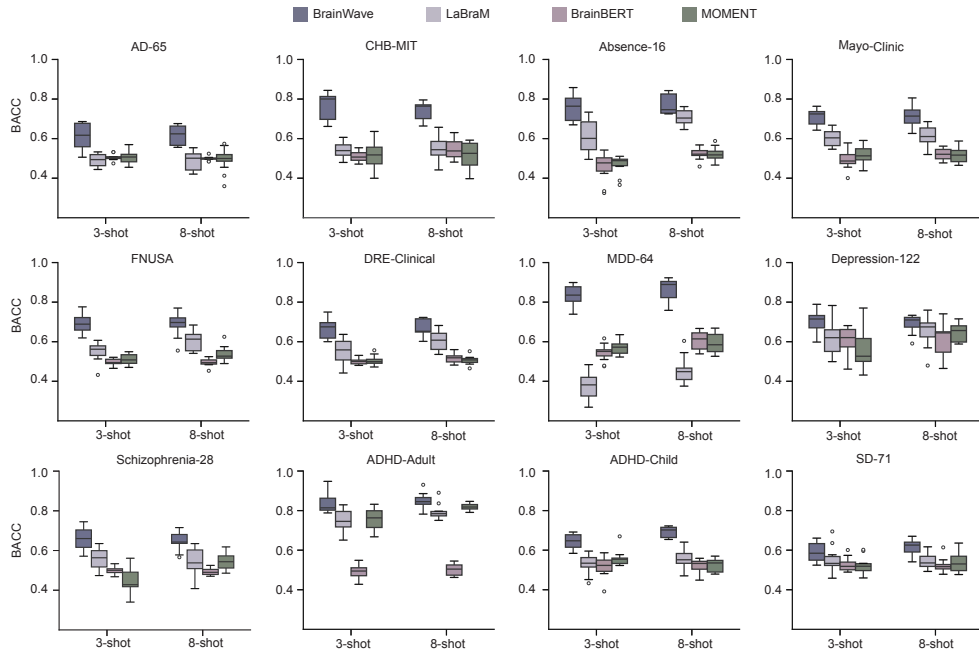


Fig. A3 Performance of few-shot classification. Box plots comparing the BACC scores of BrainWave and competing models on few-shot classification. We conduct n -fold cross validation for each experiment and repeat five runs per fold. We perform 3-shot and 8-shot classification for each task.

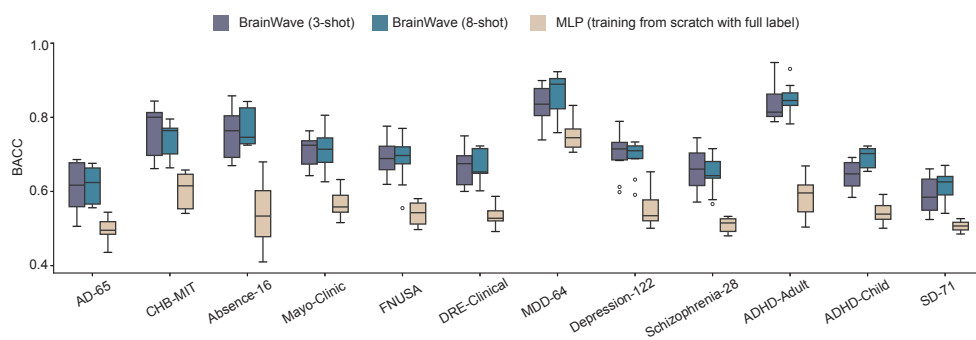


Fig. A4 Comparison between few-shot classification with BrainWave and end-to-end MLP. Box plots comparing the BACC scores of BrainWave on few-shot classification and end-to-end trained MLP with full-label supervision.

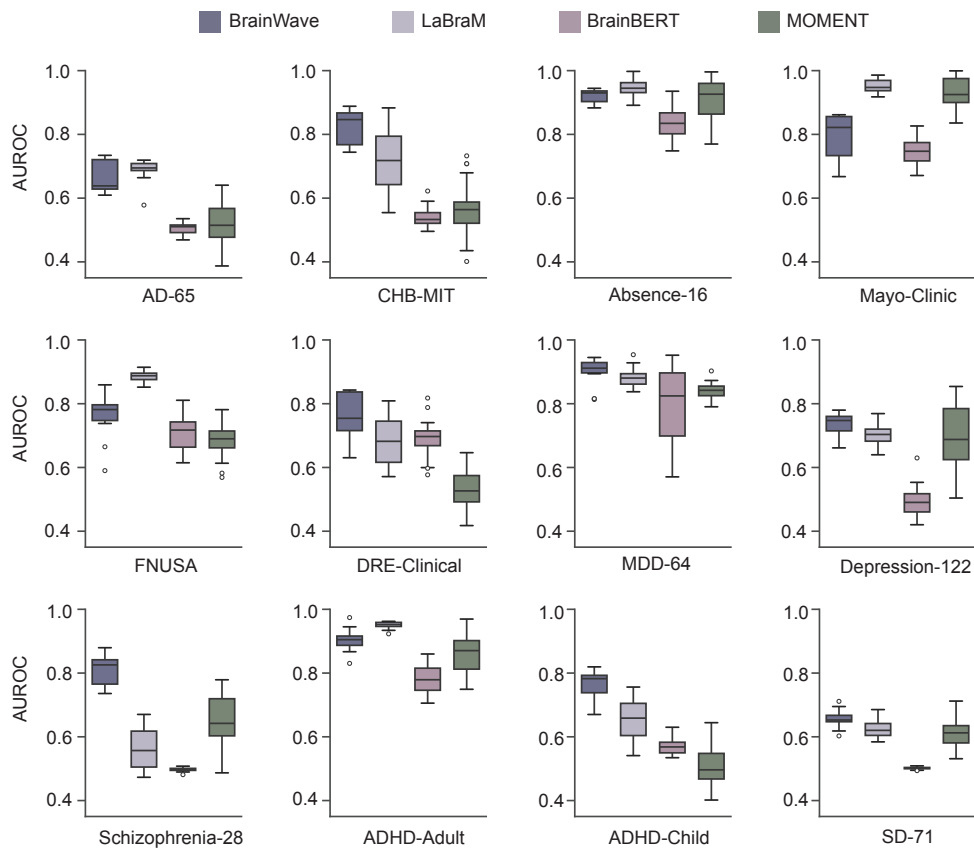


Fig. A5 Comparison between few-shot classification with BrainWave and full-label fine-tuning of competing models. Box plots comparing the AUROC scores of BrainWave on 8-shot classification and other pretrained models on full-label fine-tuning. For all the models, we conduct n -fold cross validation in each experiment and repeat five runs per fold.

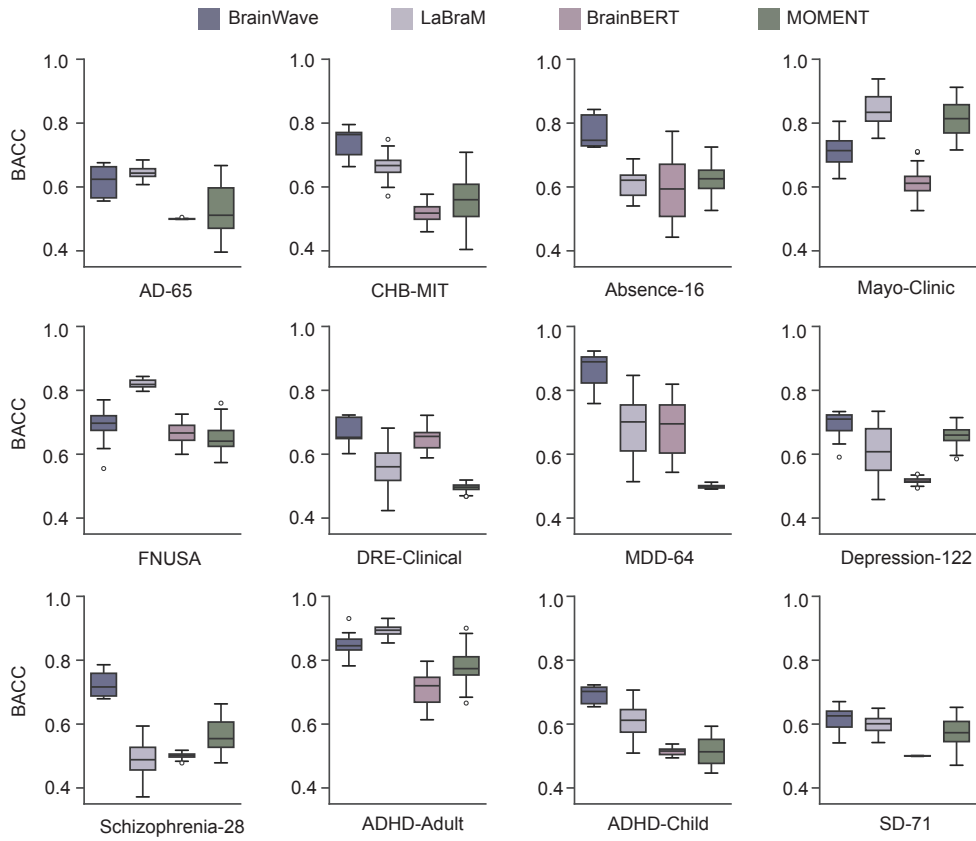


Fig. A6 Comparison between few-shot classification with BrainWave and full-label fine-tuning of competing models. Box plots comparing the AUROC scores of BrainWave on 8-shot classification and other pretrained models on full-label fine-tuning. For all the models, we conduct n -fold cross validation in each experiment and repeat five runs per fold.

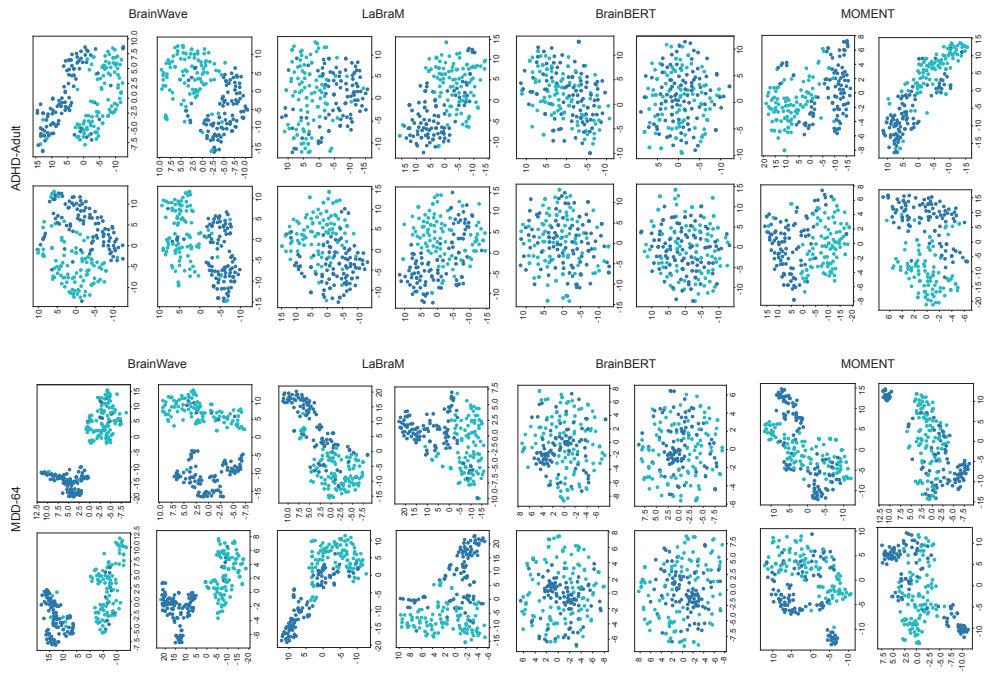


Fig. A7 t-SNE analysis of few-shot classification. t-SNE plots of the pre-trained representations on ADHD-Adult and MDD-64 generated from BrainWave and other pre-trained encoders. Each model contains four subplots, with each subplot generated by randomly sampling a portion of the original dataset.

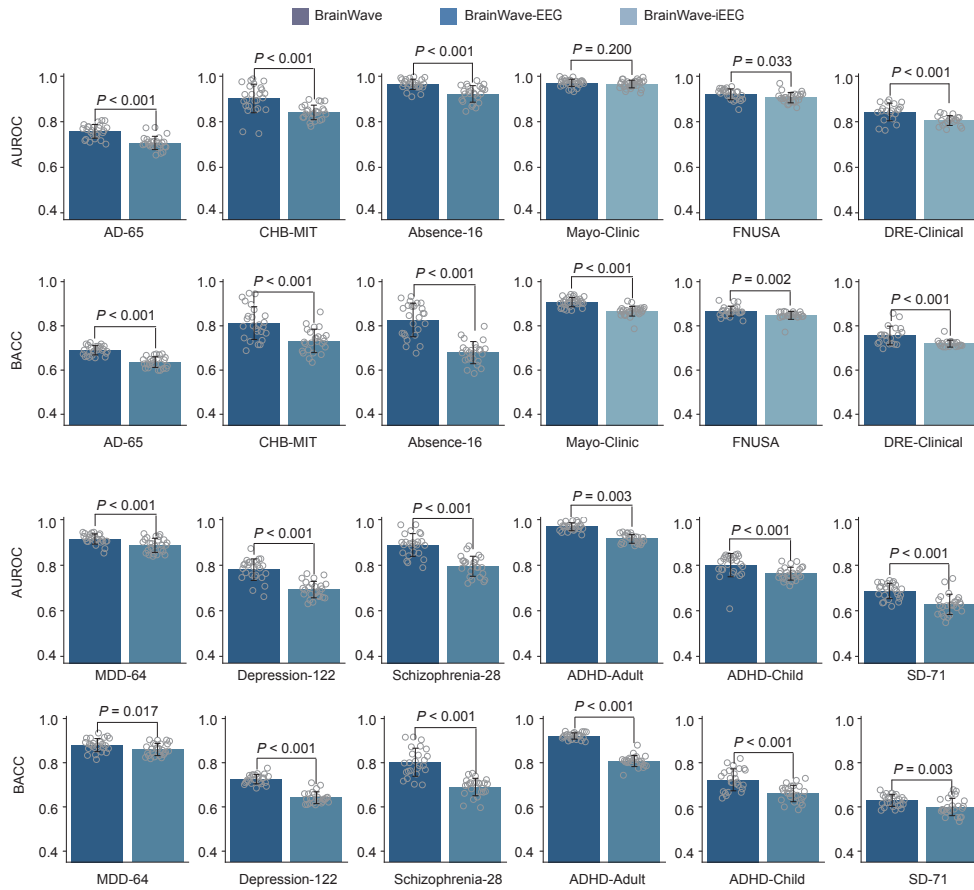


Fig. A8 Performance of cross-subject evaluation with BrainWave, BrainWave-EEG and BrainWave-iEEG. Bar plots comparing the AUROC and BACC scores of BrainWave, BrainWave-EEG and BrainWave-iEEG on cross-subject tasks. Each experiment is conducted with n -fold cross validation (n is the number of subject groups), where we repeat five runs for each fold.

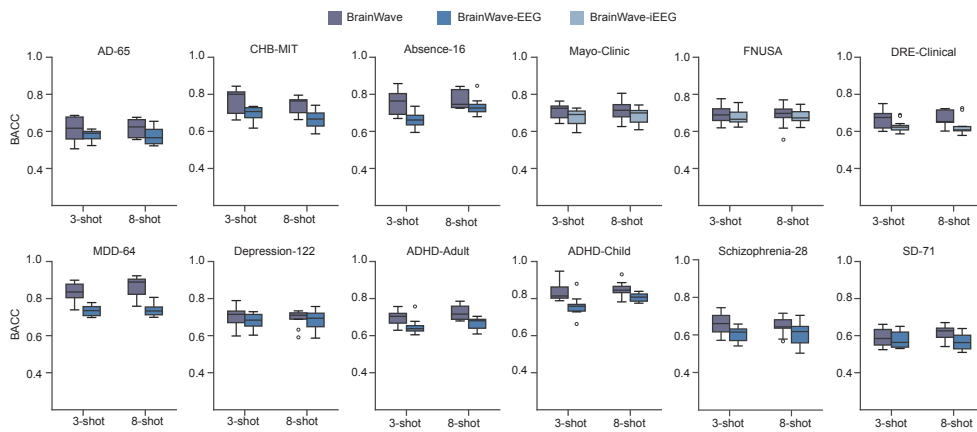


Fig. A9 Performance of few-shot classification with BrainWave, BrainWave-EEG and BrainWave-iEEG. Box plots comparing the BACC scores of BrainWave, BrainWave-EEG and BrainWave-iEEG on few-shot classification. We perform 3-shot and 8-shot classification for each task. Data are mean \pm SD. The listed p value indicates the significance for BrainWave outperforming the best comparison model, with the two-sided t -test.

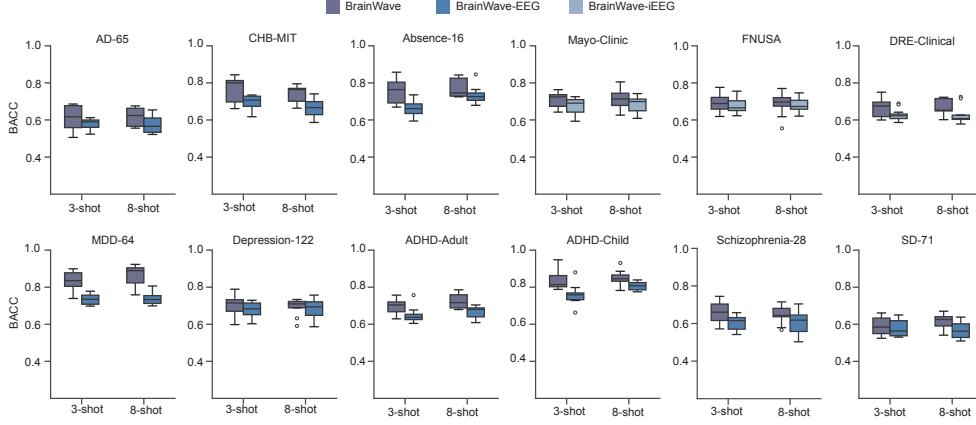


Fig. A10 Performance of few-shot classification with BrainWave, BrainWave-EEG and BrainWave-iEEG. Box plots comparing the BACC scores of BrainWave, BrainWave-EEG and BrainWave-iEEG on few-shot classification. We perform 3-shot and 8-shot classification for each task. Data are mean \pm SD. The listed p value indicates the significance for BrainWave outperforming the best comparison model, with the two-sided t -test.

Appendix B Supplementary Notes

B.1 Overview of Different Foundation Models

Table B1 Comparison of BrainWave and other competing models in terms of scope, pretraining data, data duration and number of pretraining patches.

Model	Scope	Pretraining data	Data duration (hours)	# of patches (billion)
LaBraM	Brain signal	EEG	2534.8	-
BrainBERT	Brain signal	iEEG	43.7	-
MOMENT	Universal time series	Multiple domains	-	0.15
BrainWave	Brain signal	EEG + iEEG	40906.5	3.16

B.2 Pretraining Datasets

Table B2 Statistics of datasets used for pretraining. The pretraining corpus for BrainWave contains more than 40,000 hours of electrical brain recordings collected from about 16,000 individuals.

Dataset	Data type	# of subjects	Data volume (GB)	Duration (hours)	Sampling rate (Hz)	# of channels
CAP	EEG	108	40.1	505	100	5-13
HMC	EEG	151	15.7	1144	256	4
Siena	EEG	14	20.3	141	512	27
SRM	EEG	111	4.49	9	1024	64
TUEG	EEG	14987	1643	27063	250-512	23
Schizophrenia-81	EEG	81	20.8	19	1024	64
Sleep-EDF	EEG	107	8.1	1661	100	1
Stroke-50	EEG	50	2.18	4	500	29
PD-31	EEG	31	0.545	2	512	32
IowaDataset	EEG	28	7.6	5	500	10
UNMDataset	EEG	54				
AD-184	EEG	184	0.007	0.5	128	21
private-EEG	EEG	16	1470.17	5122	1000-2000	8-36
CCEP	iEEG	74	269.11	89	2048	48-116
private-iEEG	iEEG	17	10618.68	5142	1000-4096	75-238

B.3 Evaluation Datasets

Table B3 Evaluation dataset DRE-Clinical: number of samples included in each subject group for each class. Each sample is a 20-second, single-channel data segment.

Subject group id	# of Normal samples	# of Seizure samples
0	37970	7594
1	54325	10865
2	24865	4973
3	74450	14890

Table B4 Evaluation dataset Absence-16: number of samples included in each subject group for each class. Each sample is a 4-second, 19-channel data segment.

Subject group id	# of Normal samples	# of Seizure samples	# of IED samples
0	1402	67	33
1	1724	80	68
2	1648	85	27
3	1073	100	50
4	1539	76	44

Table B5 Evaluation dataset Clonic-6: number of samples for each class. Each sample is a 4-second, 19-channel data segment.

# of Normal samples	# of Seizure samples	# of IED samples
1130	223	563

Table B6 Evaluation dataset Atonic-5: number of samples for each class. Each sample is a 4-second, 19-channel data segment.

# of Normal samples	# of Seizure samples	# of IED samples
1188	285	114

Table B7 Evaluation dataset AD-65: number of samples included in each subject group for each class. Each sample is a 10-second, 19-channel data segment.

Subject group id	# of Control samples	# of AD samples
0	504	671
1	512	529
2	491	578
3	489	564
4	431	580

Table B8 Evaluation dataset CHB-MIT: number of samples included in each subject group for each class. Each sample is a 10-second, 23-channel data segment.

Subject group id	# of Normal samples	# of Seizure samples
0	738	246
1	624	208
2	987	329
3	294	98
4	468	156

Table B9 Evaluation dataset Mayo-Clinic: number of samples included in each subject group for each class. Each sample is a 3-second, single-channel data segment.

Subject group id	# of Normal samples	# of Seizure samples
0	7531	3432
1	15006	883
2	12326	1923
3	10951	2747
4	38824	2816
5	13394	3426

Table B10 Evaluation dataset FNUSA: number of samples included in each subject group for each class. Each sample is a 3-second, single-channel data segment.

Subject group id	# of Normal samples	# of Seizure samples
0	10511	3439
1	48035	15786
2	19768	10949
3	28299	6156
4	20546	16140

Table B11 Evaluation dataset MDD-64: number of samples included in each subject group for each class. Each sample is a 10-second, 19-channel data segment.

Subject group id	# of Normal samples	# of MDD samples
0	730	857
1	639	824
2	639	809
3	714	733
4	694	670

Table B12 Evaluation dataset Depression-122: number of samples included in each subject group for each class. Each sample is a 10-second, 64-channel data segment.

Subject group id	# of Control samples	# of Depression samples
0	747	440
1	720	440
2	737	424
3	742	445
4	696	445

Table B13 Evaluation dataset Schizophrenia-28: number of samples included in each subject group for each class. Each sample is a 10-second, 19-channel data segment.

Subject group id	# of Control samples	# of Schizophrenia samples
0	588	595
1	540	686
2	541	637
3	558	782
4	365	452

Table B14 Evaluation dataset ADHD-Adult: number of samples included in each subject group for each class. Each sample is a 5-second, 2-channel data segment.

Subject group id	# of Control samples	# of ADHD samples
0	576	512
1	576	512
2	512	448
3	512	448
4	512	448

Table B15 Evaluation dataset ADHD-Child: number of samples included in each subject group for each class. Each sample is a 5-second, 19-channel data segment.

Subject group id	# of Control samples	# of ADHD samples
0	278	386
1	258	375
2	299	327
3	341	424
4	289	345

Table B16 Evaluation dataset SD-71: number of samples included in each subject group for each class. Each sample is a 5-second, 61-channel data segment.

Subject group id	# of Control samples	# of Deprivation samples
0	1380	1392
1	1560	1560
2	1249	1187
3	1140	1080
4	1080	14975

Table B17 Evaluation dataset Apnea-ECG: number of samples included in each subject group for each class. Each sample is a 60-second single-channel data segment.

Subject group id	# of Normal samples	# of Apnea samples
0	4371	2302
1	4408	2390
2	3950	2990
3	4223	2688
4	4261	2688

B.4 Configurations

Table B18 Pretraining configurations of BrainWave.

Hyperparameter	Value
Optimizer	AdamW
Optimizer momentum	$\beta_1 = 0.9, \beta_2 = 0.95$
Learning rate schedule	linear warmup with cosine decay
Max learning rate	1×10^{-5}
Warmup step	1000
Decay step	15600
Global batch size	2560000 signal patches
Max context length	60 seconds

Table B19 Model configurations of BrainWave.

Hyperparameter	Value
Hidden size	768
Intermediate size	2048
# of layer	10
# of attention head in Transformer encoder	16
# of attention head in channel attention	16
Position embedding	absolute
Hidden activate	GELU

B.5 Supplementary Results

Table B20 Table comparing the number of principal components k that explains 99% of the variance of each EEG dataset.

Dataset	BrainWave	BrainWave-EEG
AD-65	65	30
CHB-MIT	34	16
Absence-16	63	27
Clonic-6	66	26
Atonic-5	58	18
MDD-64	31	19
Depression-122	5	7
Schizophrenia-28	79	24
ADHD-Adult	114	49
ADHD-Child	39	29
SD-71	8	5

Table B21 Table comparing the number of principal components k that explains 99% of the variance of each iEEG dataset.

Dataset	BrainWave	BrainWave-iEEG
Mayo-Clinic	36	28
FNUSA	37	22
DRE-Clinical	67	55